

## Continuous, dense, highly collimated sodium beam

W. DeGraffenreid,<sup>a)</sup> J. Ramirez-Serrano, Y.-M. Liu,<sup>b)</sup> and J. Weiner<sup>c)</sup>

Laboratory for Atomic, Molecular, and Optical Science and Engineering, University of Maryland, College Park, Maryland 20742

(Received 28 March 2000; accepted for publication 28 June 2000)

We have developed a slow, highly collimated, and bright sodium atom beam suitable for orientation and alignment studies in cold collisions. A combination of transverse-optical collimation, longitudinal cooling, rapid decoupling from the longitudinal cooling cycle, and a final “optical-force extrusion” stage produces an atom density of  $1 \times 10^{10} \text{ cm}^{-3}$  within a beam-divergence solid angle of  $2 \times 10^{-6} \text{ sr}$ . Rapid Zeeman-cooler decoupling results in a narrow laboratory velocity distribution of 5 m/s full width at half maximum and a cold binary intrabeam collision temperature of 4 mK. © 2000 American Institute of Physics. [S0034-6748(00)02110-9]

### I. INTRODUCTION

In recent years much effort has been devoted to high-performance atom-beam sources. Because of the dissipative nature of the “radiation pressure” force,<sup>1</sup> optically cooled and compressed atom beams can achieve brightness figures (flux density per unit solid angle) well beyond the Liouville-theorem limit.<sup>2</sup> Bright beams are useful in improving the efficiency of the loading of optical traps, for nanolithography, atom interferometry; and, in the case of interest here, cold collision studies.

A variety of techniques have been developed over the last decade that use optical forces to generate bright beams. Some of these techniques start with a cold or ultracold ensemble of atoms and generate a beam by breaking the symmetry of the confinement.<sup>3–7</sup> Other schemes start with a hot thermal beam and use optical forces to increase the brightness.<sup>8–14</sup> Here, we present a multistage system which renders a continuous thermal source into a continuous cold beam suitable for atomic collision studies. After discussing the diagnostic techniques used to characterize the beam, it will be compared to several other bright atom beams.

While the rate constants of cold and ultracold collisions can be measured in the “reaction bulb” environment of a magneto-optic trap (MOT),<sup>15</sup> the isotropic distribution of collision axes limits these studies to spatially averaged quantities. However, in the cold collision regime, where only a few partial waves participate, is just where alignment and orientation effects can be especially pronounced. A highly collimated atom beam, therefore, provides an ideal environment for studying favorable classes of collision kinematics. In particular, inelastic or reactive processes proceeding through a two-step interaction sequence, the first occurring at long range and the second at short range, results in a very narrow acceptance angle along the *molecular* axis of the ap-

proaching atoms. Examples of these kinds of collisions are photoassociative ionization<sup>15</sup> and harpooning collisions.<sup>16</sup> If the laboratory divergence angle of the atom beam is also highly restricted, the molecular collision axis nearly superposes on the *laboratory* axis, providing a collision reference axis accessible to laboratory manipulation.

In this work, the combination of a simple effusive source, optical collimation, Zeeman cooling, and a simple technique for sharply decoupling the atoms from the cooling cycle generates a bright beam. Under typical conditions, we obtain a sodium beam with  $1 \times 10^{10} \text{ atoms cm}^{-3}$  in a solid angle of  $2 \times 10^{-6} \text{ sr}$  with a longitudinal laboratory velocity of  $\sim 350 \text{ m/s}$  and velocity spread of 5 m/s. This beam has been used to perform studies of the polarization dependence of the optical suppression of photoassociation ionization collisions in sodium<sup>17</sup> and of the polarization dependence of photoassociation.<sup>18</sup>

### II. BEAM PRODUCTION

We use a multistep process to generate the beam, with each element discussed in some detail below. Figure 1(a) sketches the production of the beam with elements scaled individually and the vacuum chamber removed for clarity, while Fig. 1(b) is a scaled diagram of the complete system.

#### A. Thermal source

An externally heated oven assembled primarily from off-the-shelf UHV components generates the thermal beam. High-temperature custom-fitted mantles (Glascol, Terre Haute, IN) heat sodium metal inside a reservoir made from a standard 4.5-in.-diam CF tee to about 400 °C. The reservoir mates to a standard six-way CF cross. A thin stainless-steel disk with a centered 1.25-mm-diam hole was welded into the entrance arm of the six-way cross. This aperture acts as a nozzle for the existing atom flux from the reservoir. A 1.25-mm-diam skimmer aperture, formed from a similar stainless-steel disk welded into the arm opposite the nozzle and positioned 16 cm downstream, mechanically defines and precollimates the metal vapor flux. The mounting of the nozzle and skimmer within the same six-way CF cross de-

<sup>a)</sup>Electronic mail: degraff@annick2.umd.edu

<sup>b)</sup>Permanent address: Department of Modern Applied Physics, Tsinghua University, Beijing 100084, China.

<sup>c)</sup>Also at: Laboratoire des Collisions, Agrégats, et Réactivité, IRSAMC, Université Paul Sabatier, 118 route de Narbonne, 311062 Toulouse, France.

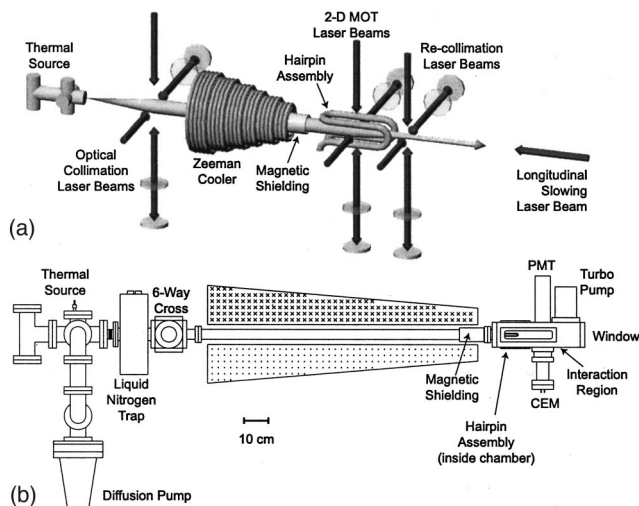


FIG. 1. (a) Sketch of technique used to produce the cold, bright beam. A thermal source produces a flux that is optically collimated and longitudinally cooled. After extraction from the longitudinal cooling cycle with a high magnetic-field gradient, the atoms are extruded into a narrow, dense atom beam with a two-step compression and recollimation stage. The high vacuum chamber has been removed for clarity. (b) Scaled diagram of experimental setup.

finishes a stable and rigid atom-beam axis. A separate heating mantle enveloping the cross heats the nozzle and skimmer to  $400\text{ }^{\circ}\text{C}$  to prevent clogging. A diffusion pump (nominal 4 in. diam with pumping speed 800 l/s) removes the skimmed sodium vapor from the region between the nozzle and skimmer. A coiled solenoidal structure surrounding the atom-beam axis and formed from 3/16-in.-diam commercial copper refrigeration tubing increases the pumping speed between nozzle and skimmer by acting as a primitive cryopump. It is introduced through the top arm of the cross. Simply running cold tap water in this cooling coil suffices due to the low vapor pressure of sodium at or slightly below ambient temperature ( $\sim 10^{-10}$  Torr at  $25\text{ }^{\circ}\text{C}$ ). Figure 2 shows a cutaway view of the beam source. The skimmer–nozzle configuration mechanically restricts the atomic beam to a divergence angle of 8 mrad. The longitudinal velocity components (along the axis defined by the assembly) of the flux exiting the nozzle are below 1500 m/s. Therefore, the 16 cm distance from the nozzle to skimmer, together with the diameter of the holes, limits the transverse component, which clears the skimmer to less than 10 m/s. The beam source is connected to the main chamber by a flexible bellows which provides adjustment of the beam pointing. An annular-shaped liquid-nitrogen trap with a hole diameter of 7.5 mm separates the collimation region from the longitudinal Zeeman cooling tube, providing further isolation of the downstream stages from background sodium vapor.

Mounting the sodium source external to the main vacuum chamber and surrounding it with the custom-fitted heating mantles provides a major benefit of uniform source temperature. Wrapping the heating mantles with aluminum foil and several layers of fiberglass tape distributes the heat evenly around the oven and prevents turbulent instabilities in the beam flux. Another benefit of the external source is the ease with which the reservoir is recharged. The top flange on

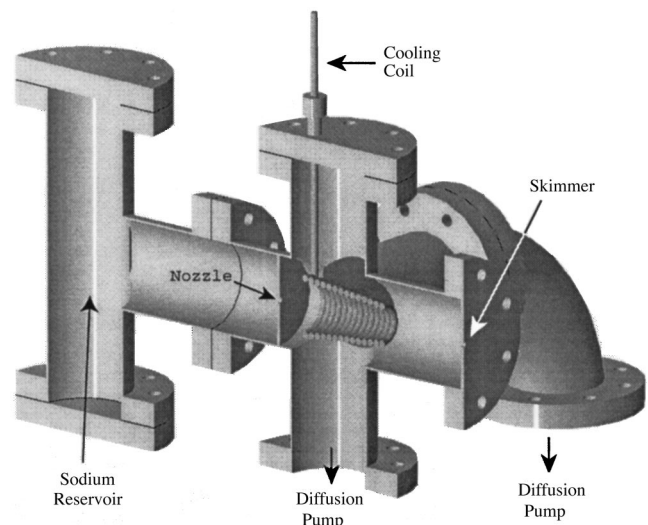


FIG. 2. Externally heated source for generation of thermal sodium beam in cutaway. Nozzle and skimmer are mounted coaxially within a six-way cross. Between the nozzle and skimmer, excess flux is pumped away on three sides by a diffusion pump aided by additional pumping from a coaxial cooling coil with cold water running through it. Custom-shaped heating mantles surround the tee and cross and heat the oven to  $400\text{ }^{\circ}\text{C}$ .

the tee is removed and small lumps of sodium metal are dropped in.

## B. Optical collimation

Optical molasses<sup>1</sup> collimates the sodium beam by cooling the transverse velocity of the atoms. A pair of counter-propagating laser beams, orthogonal to the atom beam and tuned about one natural linewidth to the red of the atomic resonance, impinges on the atom-beam flux. Atoms preferentially absorb from the laser beam toward which they are moving because the light frequency is Doppler shifted closer to the atomic resonance. When an atom absorbs, it slows because of the momentum transfer from the photon. Spontaneous decay from the excited state also produces a momentum recoil, but it averages to zero over several absorptions due to the isotropic distribution of the reemitted photon. The average total momentum transferred to the atom per absorption cycle, therefore, equals the momentum of a single photon  $\hbar\mathbf{k}$ , where  $|k| = 2\pi/\lambda$ . The force resulting from the momentum transfer always opposes the motion of the atoms and to first order is proportional to the atom velocity, creating a damping term in the equation of motion. Two pairs of counter-propagating laser beams, orthogonal to each other as well as to the atom beam, damp the transverse velocity components along two axes.

In the simplest theory of optical cooling, two-level Doppler cooling, the temperature limit is reached when the rate of heating due to the random motion from spontaneous emission equals the cooling rate. This limit is given by  $T_D = \hbar\Gamma/2k_B$ ,<sup>1</sup> where  $\Gamma$  is the natural linewidth of the transition (and equal to  $1/\tau$ , where  $\tau$  is the excited-state lifetime). For sodium, the Doppler temperature equals  $240\text{ }\mu\text{K}$ , corresponding to an average velocity  $v_D$  of 41 cm/s ( $k_B T_D = \frac{1}{2}mv_D^2$ ). However, additional sub-Doppler damping mechanisms exist that further cool the ensemble to tempera-



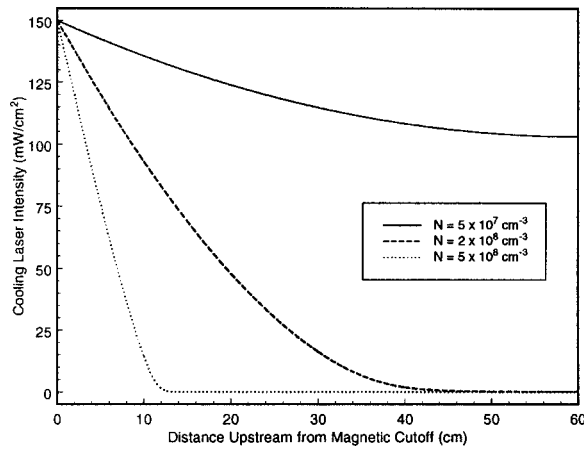


FIG. 4. Cooling laser intensity as a function of position upstream from the magnetic cutoff for several ground-state densities. For densities above  $2 \times 10^8 \text{ cm}^{-3}$ , the slowing laser becomes strongly attenuated at the upstream end of the Zeeman cooler.

the hyperfine splitting. Many turns of 0.25-in.-diam commercial refrigeration tubing form our solenoid. The total current of 60 A that runs through the solenoid is provided by a high-current power supply (Sorenson, DCR 80-125T). Heat generated resistively in the solenoid is removed by water flowing through the tubing.

As the atoms enter the upstream end of the Zeeman cooler, the energy levels of the atoms shift due to the Zeeman effect. A Spectra Physics 380D ring dye laser, pumped by a Coherent 25 W Sabre argon-ion laser, provides the light used for longitudinal cooling. Atoms move freely down the cooler until the Doppler-shifted frequency of the laser equals the field-dependent  $^2S(F=2, M_F=2) \rightarrow ^2P(F=3, M_F=3)$  transition energy. The resonant condition for atoms with longitudinal velocity  $v_{\parallel}$  is

$$\Delta - \mathbf{k}_L \cdot \mathbf{v}_{\parallel} + \frac{\mu_B B}{\hbar} = 0, \quad (1)$$

where  $B$  is the local magnetic field and  $\mu_B$  is the Zeeman constant for the transition ( $2\pi \cdot 1.4 \text{ MHz/G}$  for this transition). Once resonant, the atoms continue to decelerate, and slower atoms enter the cycle as the flux proceeds down the cooler.<sup>21</sup> The cooling laser is typically detuned 200 MHz below the atomic resonance with an intensity of  $150 \text{ mW/cm}^2$  at the entrance of the vacuum chamber.

The increased density of the atom beam due to the collimation increases the optical thickness of the sodium beam. We developed a crude two-level model that calculates the intensity of the cooling laser as a function of position, taking into account the absorption of photons from the cooling laser by resonant atoms. We used a spatially dependent ground-state distribution to model the resonant absorbing ground-state population determined by the combination of the varying Doppler and Zeeman shifts. The model indicates that when the ground-state density exceeds  $2 \times 10^8 \text{ atoms/cm}^3$ , the intensity falls below the saturation intensity ( $I_0 = 6 \text{ mW/cm}^2$ ) for the cooling transition at the upstream end of the cooling region. Figure 4 shows the intensity of the cooling laser for several ground-state densities as a function of distance upstream from the cooling cutoff. Low laser in-

tensity at the upstream end of the Zeeman slower inhibits efficient cooling of the fastest atoms (there will always be a fraction of uncooled atoms in the high-velocity tail of the thermal distribution that are not captured in the cooling cycle). To increase the intensity of the cooling laser at the upstream end, we focus the laser beam with a pair of lenses in a “near-telescope” configuration which overcomes the loss in cooling-laser photon flux by decreasing the laser beam cross section. The focus of the cooling laser is adjusted with the lenses to get the highest flux of cooled atoms at the exit of the solenoid.

#### D. Magnetic cutoff

Cold collision studies require low *relative* velocities ( $< 5 \text{ m/s}$ ) between pairs of atoms. To produce an ensemble of coaxially moving atoms with small relative speed, the laboratory distribution of velocities must be narrow. Slowing the atoms to near-zero velocity in the laboratory frame actually increases the distribution because the magnetic field at the end of the tapered solenoid does not exactly match the field shape needed for cooling. Rapid removal from the cooling cycle at a well-defined velocity upstream from the end of the solenoid produces an atom beam with a narrow longitudinal velocity spread. Atoms will exit the cooling cycle<sup>22</sup> if the field gradient exceeds

$$\left| \frac{dB}{dz} \right|_{\text{crit}} = \frac{1}{v_{0,\parallel}} \frac{\hbar |\mathbf{k}|^2}{2\tau\mu_B m} \frac{S}{S+1}, \quad (2)$$

where  $v_{0,\parallel}$  is the longitudinal atom velocity at the decoupling point,  $\tau$  is the excited-state lifetime,  $\mu_B$  is the Zeeman constant,  $m$  is the sodium atomic mass, and  $S$  is the saturation parameter ( $=I/I_0$ ) with  $I_0$  the resonance transition saturation power density. We tailor the magnetic field with an assembly of magnetic shielding. Multiple layers of a high-permeability nickel alloy foil (available from industrial distributors such as McMaster-Carr), wrapped into a cylindrical tube 10 cm in length and wall thickness of 2 mm, from the assembly. The structure, mounted coaxially with the atom beam and within the downstream end of the solenoid, shields the atoms from the Zeeman cooling field, as shown in Fig. 5. The terminal longitudinal velocity is determined by the resonant condition [Eq. (1)] at the site of decoupling. For the experimental conditions described here, the gradient increases to a maximum value of  $140 \text{ G/cm}$  at the edge of the shielding, well above the critical value of  $30 \text{ G/cm}$  given by Eq. (2), and atoms decouple from the cooling cycle with a velocity  $v_{\parallel}$  of  $350 \text{ m/s}$ . Using the velocity characterization technique described below, we measure the laboratory frame longitudinal velocity dispersion  $\Delta v_{\parallel}$  to be  $5 \text{ m/s}$ .

To vary the terminal velocity of the atoms, several techniques can be used to change the resonant condition given by Eq. (1). Perhaps the most straightforward method is to change the detuning of the laser. If the laser is tuned closer to the atomic resonance, the terminal velocity decreases. The magnetic-field strength varies with the solenoid current; decreasing the current will also lower the terminal velocity. Shifting the position of the shielding assembly also can be used to tune the atomic velocity by changing the decoupling

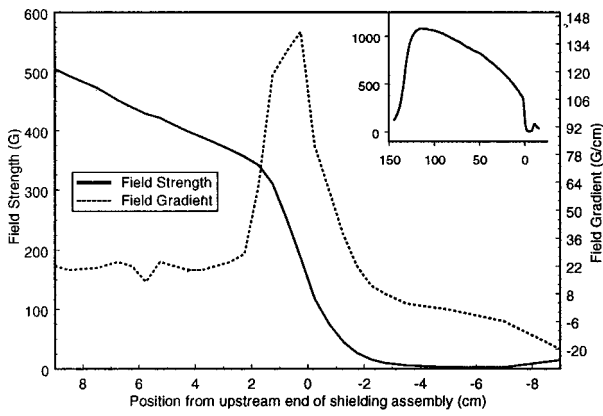


FIG. 5. Magnetic field and magnetic-field gradient in the vicinity of magnetic shielding. The magnetic shielding rapidly cuts off the Zeeman cooling field, increasing the gradient above the critical limit given by Eq. (2) for adiabatic following. Atoms are rapidly decoupled from the cooling cycle at this location, yielding a narrow longitudinal velocity distribution. The inset shows the field profile over the length of the solenoid.

point. The terminal atomic velocity can be shifted over a range of several hundred m/s using different combinations of these techniques.

### E. Extruder

To further increase the brightness of the atom beam, the flux must be compressed into a smaller volume, without increasing the divergence of the beam at the same time. A two-step process, utilizing a focusing step followed by optical collimation, reduces the beam diameter from 2 to 0.6 mm without loss of atom-beam collimation.

The focusing stage of the extruder is a two-dimensional magneto-optic trap (2D MOT).<sup>23</sup> Like optical molasses, a 2D MOT has counterpropagating pairs of laser beams, of frequency  $\omega_L$ , tuned to the red of atomic resonance  $\omega_0$  by an amount  $\Delta = \omega_L - \omega_0$ , but also includes a uniform quadrupole magnetic field aligned along the atom-beam axis. The magnetic field increases radially from the quadrupole axis and adds a Zeeman shift to the atomic levels. The force exerted on the atoms for a pair of counterpropagating laser beams is  $\mathbf{F} = \mathbf{F}_+ + \mathbf{F}_-$ , where

$$\mathbf{F}_{\pm} = \pm \frac{\hbar \mathbf{k} \Gamma}{2} \frac{S}{1 + S + \left[ \frac{2}{\Gamma} \left( \Delta \mp \mathbf{k} \cdot \mathbf{v} \pm \mu_B \frac{dB}{dr} r \right) \right]^2}. \quad (3)$$

Two sets of counterpropagating laser beams generate a cylindrical, damped restoring force that drives the atoms towards the field zero along the beam axis. Figure 6 shows the force as a function of radial position for atoms with  $v_{\perp} = 0$ , a saturation parameter  $S$  of 10, and laser detuning  $\Delta = -15$  MHz for field gradients of 40 and 80 G/cm. To calculate the force, we convert the detuning into angular frequency ( $\Delta' = \Delta \cdot 2\pi$ ) for consistency in units.

A hairpin assembly generates the extruder magnetic field. Four sections of wires, with alternating directions of current, formed from a single piece of 8 AWG solid copper wire, produce the quadrupole field. The aluminum structure used to support and mount the wire inside the vacuum chamber is not shown in Fig. 1 for clarity. The straight sections of

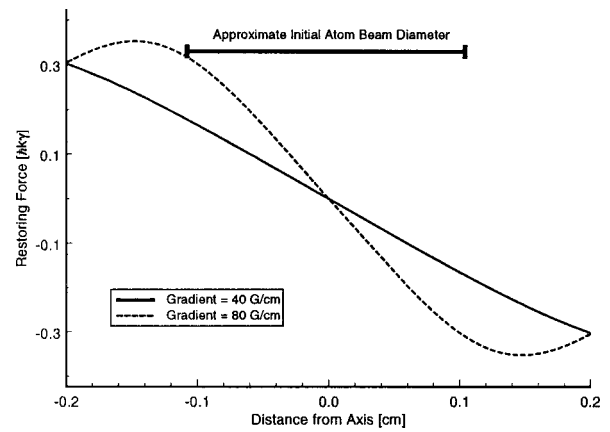


FIG. 6. MOT restoring force as a function of position for 40 and 80 G/cm for atoms with  $v_{\perp} = 0$ . The bar above the force curves shows the approximate diameter of the atom beam when it enters the 2D MOT.

wire are 5 cm long and 1 cm offset from nearest neighbors. High-current feedthroughs direct the current into and out of the vacuum chamber. A high-current supply (Sorenson, DCR 160-62T) provides the 30–50 A used to focus the atom beam. Similar to the upstream end of the Zeeman cooler, a pair of coaxial Helmholtz coils cancels the fringing fields from the solenoid. As shown in Fig. 6, the restoring force exerted on the atoms within the beam radius ( $|r| \leq 0.1$  cm) increases with the field gradient, which is proportional to the hairpin current.

The light used for the 2D MOT originates from the same Coherent 899-21 ring dye laser as the optical collimation, tuned 15 MHz to the red of the atomic resonance. A telescope expands the laser-beam diameter to 2 cm. After passing through a quarter-wave plate that converts the polarization from linear to circular, a beamsplitter divides the light into two equal intensity beams ( $55$  mW/cm<sup>2</sup>). The beams enter the chamber perpendicular to each other, as well as to the atom beam, through the center of the clear apertures of the hairpin. After exiting the chamber, the beam passes through a quarter-wave plate before retroreflection. The double pass through the wave plate changes the handedness of the circular polarization of the laser beam as needed for MOT operation.

The 2D MOT focuses the atom beam to a point downstream from the extruder assembly. The exact focal point depends on the field gradient and on the longitudinal velocity of the beam. A broadened velocity distribution widens the focal region of the beam as the fastest atoms focus to a point more distant than the slower ones due to the shortened interaction time, analogous to chromatic aberration in geometric optics. The narrow velocity distribution produced by the rapid cutoff of the longitudinal Zeeman magnetic field results in a small focal length ( $\sim 1$  mm). For a beam with  $v_{\parallel} = 350$  m/s and a hairpin current of 45 A, the focal point is about 6 cm downstream from the 2D-MOT laser beams, as seen in Fig. 7.

To prevent atom-beam divergence beyond the focal point, an optical recollimation stage introduced at the focus damps out the transverse velocity. The lin $\perp$ lin optical molasses stage, using light produced by the same laser as the pri-

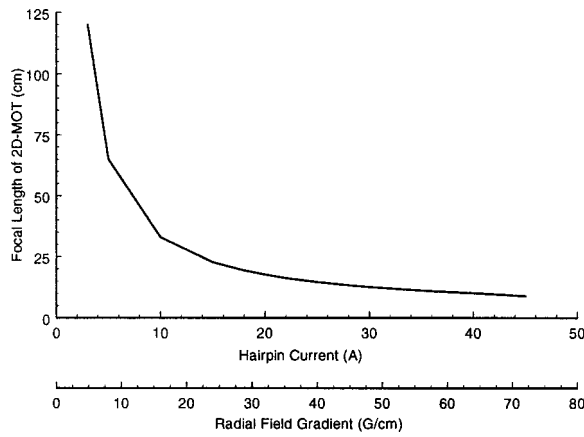


FIG. 7. Focal length of the 2D MOT as a function of current flowing through hairpin assembly for atoms with  $v_{\parallel} = 350$  m/s. The second  $x$  axis also shows the field a gradient for a given current.

mary optical collimation and the 2D MOT, is 2 cm in length and positioned at the focus of the atom beam. The same Helmholtz coils used to cancel the fringe fields in the focusing stage also cancel the magnetic field at the collimation stage to  $|B| < 1$  G, allowing sub-Doppler cooling mechanisms in the molasses to reduce the transverse temperature to  $T_{\perp} \sim 55 \mu\text{K}$ , below the Doppler limit ( $T_D = 240 \mu\text{K}$ ). The extruder acts essentially as an atom-beam telescope, reducing the beam radius  $\Delta r$  from 1 mm at the end of the Zeeman cooler to 0.3 mm at the extruder exit, based on measurements of the beam fluorescence collected with a charge-coupled-device (CCD) camera. The beam current  $J$  (atoms  $\text{s}^{-1}$ ) entering the extruder equals the exiting current, indicating that essentially all atoms are forced into the narrowed beam.

### F. Performance

We measure the performance of the beam at a point located 2.2 m downstream from the nozzle at the point where our cold collisions are detected. Adding optical collimation to the longitudinally cooled beam increases the density from  $2 \times 10^7$  to  $7 \times 10^8 \text{ cm}^{-3}$ . The extruder further increases the density to  $1 \times 10^{10} \text{ cm}^{-3}$ , a 500-fold density gain. The beam-divergence solid angle  $\Omega = \pi(\Delta v_{\perp}/v_{\parallel})^2$  decreases from  $1 \times 10^{-4}$  to  $2 \times 10^{-6} \text{ sr}$  as the thermal beam is collimated, cooled, and extruded. Table I summarizes the beam performance.

### III. DIAGNOSTICS

Here, we describe the techniques used to measure the beam size, density, and longitudinal velocity distribution. A third ring dye laser (Coherent, 899-21) provides the laser

TABLE I. Summary of beam characteristics.

$n$	Density (atoms/ $\text{cm}^3$ )	$(1 \pm 0.5) \times 10^{10}$
$v_{\parallel}$	Longitudinal velocity (m/s)	$350 \pm 5$
$\Delta v_{\parallel}$	Longitudinal velocity spread (m/s)	$5 \pm 1$
$\Delta v_{\perp}$	Transverse velocity spread (m/s)	$0.25 \pm 0.1$
$\Omega$	Solid angle (sr)	$(2 \pm 1) \times 10^{-6}$
$\Delta r$	Beam radius (cm)	$0.03 \pm 0.01$

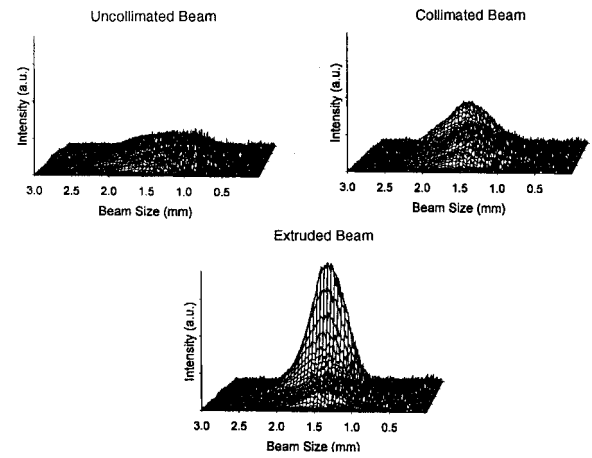


FIG. 8. Fluorescence profiles captured with a CCD camera for uncollimated, collimated, and extruded atom beams.

beams used for the diagnostics. To contrast the performance of the system to others, we introduce the definition of brightness, brilliance, and phase-space density.

### A. Beam size and density

We measure the spatial profile of the atom beam with a laser-induced fluorescence technique. Perpendicularly crossing the atom beam, a weak ( $I \sim 1 \text{ mW/cm}^2$ ), thin ribbon of light excites atoms from the  $\text{Na } ^2S(F=2)$  to the  $\text{Na } ^2P(F=3)$  level by tuning the laser to the transition. A CCD camera system (Spectrasource, Teleris 2) captures the decaying fluorescence as well as the background light. By tuning the probe laser off-resonance, we also record the background light which, after subtracting from the on-resonance image, provides a clear atom-beam profile. Figure 8 shows the fluorescence profiles for the uncollimated, collimated, and extruded cases of the longitudinally slowed atom beam. We measure the diameter of the beam, defined as the FWHM, from these images.

By measuring the absorption of a weak, resonant probe laser with circular polarization, we determine the ground-state density  $n$ . As the probe laser with initial intensity  $I_0$  passes through the atom beam with average density  $n$  and diameter  $d$ , the final intensity  $I'$  is given by

$$I' = I_0 \exp[-n \sigma_A d], \quad (4)$$

where the absorption cross section is given by

$$\sigma_A = \frac{g_e}{g_g} \lambda^2 \frac{\Gamma}{8\pi} \int_{\omega_0 - \Delta\omega_L/2}^{\omega_0 + \Delta\omega_L/2} \frac{d\omega}{(\omega - \omega_0)^2 + \left(\frac{\Gamma}{2}\right)^2}, \quad (5)$$

where  $g_e$  and  $g_g$  are the degeneracy factors for the excited and ground state,  $\lambda$  is the resonant wavelength, and  $\Delta\omega_L$  is the spectral linewidth of the laser. The circular polarization of the laser drives the stretched-state transition so that  $g_g$  and  $g_e$  equal unity. Assuming a spectral linewidth of 1 MHz from the 899-21 ring dye laser serving as the probe, the absorption cross section is  $8 \times 10^{-11} \text{ cm}^2$ . Using Eq. (5), from the measurements of the initial and final intensities

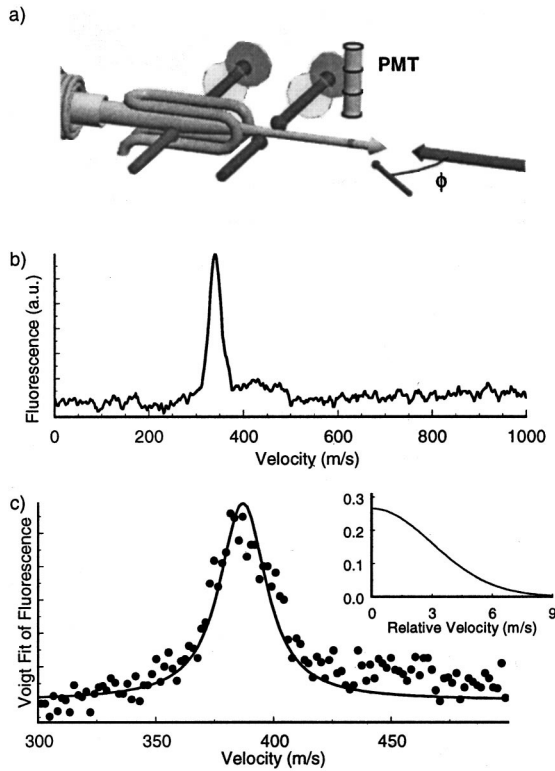


FIG. 9. Technique for calculating velocity distribution. (a) Experimental layout for laser-induced fluorescence measurement showing probe laser crossing atom beam with angle  $\phi$ . A photomultiplier collects the fluorescence. (b) Typical fluorescence profile as a function of velocity. (c) Voigt fit of fluorescence that extracts laboratory frame velocity distribution that is used to determine the relative velocity distribution (inset) for a pair of atoms.

$I_0, I'$  as well as the atom-beam diameter  $d$ , we calculate the average atom-beam density  $n$  to be  $(1 \pm 0.5) \times 10^{10} \text{ cm}^{-3}$  for an oven temperature of  $400^\circ \text{C}$ .

## B. Velocity characterization

To measure the longitudinal velocity of the atom beam, a weak probe beam ( $I < I_{\text{sat}}$ ), introduced at an angle  $\phi$  with respect to the atom beam [Fig. 9(a)], scans near the rest frame atomic resonance. The Doppler-shifted, angle-tuned resonant absorption condition is given by

$$\Delta = -\frac{v_{\parallel}}{\lambda} \cos \phi, \quad (6)$$

where  $\Delta$  is the detuning from resonance at which atoms with velocity  $v_{\parallel}$  absorb. A photomultiplier tube collects the light emitted as the atoms decay from the excited state when populated by Doppler-resonant absorption. The laser simultaneously scans across several known lines of a molecular iodine cell to provide a reference for the frequency of the laser. We convert the frequency scale of the spectra to a velocity scale by the relation given by Eq. (6) to determine the center velocity of the distribution as seen in Fig. 9(b). It is important to note that the scan shown in Fig. 9(b) includes the velocity distribution in the laboratory frame  $f(v')$  as well as the power-broadened natural linewidth projected into

velocity space  $g(v)$ . We extract the velocity distribution  $f(v')$  from the linewidth  $g(v)$ , which are of the same magnitude, by fitting a Voigt profile

$$I(v) = I_0 \int f(v') g(v - v') dv' \quad (7)$$

to the spectra. We assume a 1D Gaussian distribution of velocities for  $f(v')$ . The probe laser intensity and the center velocity of the fluorescence are known, leaving the longitudinal velocity spread  $\Delta v_{\parallel}$  and a normalization constant as the only remaining parameters to fit. A typical fit, with a laboratory velocity width  $\Delta v_{\parallel}$  equal to 5 m/s, is shown in Fig. 9(c).

The collision temperature  $T_{\text{coll}}$  for a pair of atoms depends on the relative velocity  $v_r$  between them:

$$kT_{\text{coll}} = \frac{1}{2} \mu \langle v_r \rangle^2. \quad (8)$$

An autocorrelation of the laboratory distributions,  $f(v_1)$  and  $f(v_2)$ , for two atoms

$$P(v_r) = \int_0^{\infty} \int_0^{\infty} f(v_1) f(v_2) \delta(v_r - |v_1 - v_2|) dv_1 dv_2 \quad (9)$$

extracts the relative velocity distribution  $P(v_r)$  of pairs of atoms in the beam. The inset of Fig. 9(c) shows  $P(v_r)$  for two atoms in the atom beam. We calculate the average relative velocity from the relative velocity distribution

$$\langle v_r \rangle = \int_0^{\infty} P(v_r) v_r dv_r. \quad (10)$$

For the data shown in Fig. 9, the mean relative velocity  $\langle v_r \rangle$  is 2.4 m/s and the collision temperature  $T_{\text{coll}}$  is 4 mK.

## C. Beam brightness and brilliance

Optically brightened beams have been characterized in different ways, making the comparison of performance difficult. A recent work by Lison *et al.*<sup>14</sup> defines brightness

$$R = \frac{\Phi}{\Omega}, \quad (11)$$

where  $\Phi$  is the average atomic flux and  $\Omega$  is the solid angle subtended by the beam, and brilliance

$$B = R \frac{v_{\parallel}}{\Delta v_{\parallel}} \quad (12)$$

to characterize the performance of different beams. The average atom flux  $\Phi$  ( $\text{atoms s}^{-1} \text{ m}^{-2}$ ) is the product of the density  $n$  and the longitudinal velocity  $v_{\parallel}$ . The average beam current  $J$  ( $\text{atoms s}^{-1}$ ) equals the product of the flux  $\Phi$  and the atom-beam cross-section  $\pi \Delta r^2$  and is a common measure of the number of atoms within a beam. The brilliance  $B$  measures the velocity dispersion within the beam as well as the divergence. Because cold collision studies require low longitudinal velocity dispersion, the brilliance is an important measure of the beam quality.

The performance of the atom beams is also related to the Liouville phase-space density

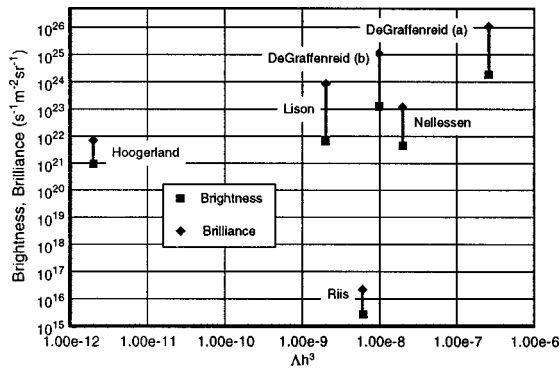


FIG. 10. Comparison of several atom beams (adapted from Ref. 14). Results are from Riis *et al.* (Ref. 3) Nellessen, Werner, and Ertmer (Ref. 8), Hoogerland *et al.* (Ref. 11), Lison *et al.* (Ref. 14), and DeGraffenreid *et al.* (a) (this work), and DeGraffenreid *et al.* (b) (this work without the extruder stage).

$$\Lambda = \frac{N}{(\Delta x \Delta p)^3}, \tag{13}$$

the number of atoms  $N$  per phase-space volume  $(\Delta x \Delta p)^3$ . It can be shown that for a cooled atom beam with cylindrical symmetry, the dimensionless phase-space density  $\tilde{\Lambda} = \Lambda h^3$  equals

$$\tilde{\Lambda} = \frac{nh^3}{m^3 \Delta v_{\perp}^2 \Delta v_{\parallel}}, \tag{14}$$

where  $m$  is the atomic mass.

The brightness and brilliance of the collimated and extruded cold atom beam are, respectively,  $(2 \pm 1) \times 10^{24}$  and  $(1 \pm 0.5) \times 10^{26} m^{-2} s^{-1} sr^{-1}$  with a dimensionless phase-space density  $\tilde{\Lambda}$  of  $(2.6 \pm 1) \times 10^{-7}$ .

#### IV. COMPARISON TO OTHER SOURCES

Figure 10 shows the brilliance and brightness of several cool atom beams as a function of the phase-space density. Here, we discuss the performance of several of these other sources: a sodium atomic funnel,<sup>3</sup> a slowed and compressed sodium beam,<sup>8</sup> a brightening scheme for metastable neon,<sup>11</sup> and a system that uses permanent magnets to both decouple atoms from a collimated, longitudinal cooled beam and to focus the atoms to a smaller beam diameter.<sup>14</sup> A recently developed system that produces a pulsed flux of lithium atoms developed by Fukuyama *et al.*<sup>7</sup> from a magneto-optic trap is also presented.

Riis *et al.*<sup>3</sup> developed an ‘‘atomic funnel’’ source, essentially a 2D MOT, with an adjustable optical molasses along the third axis. By using beams with slightly different detunings from resonance in the molasses beams, the atoms leave the funnel along this axis with a velocity  $v_z$  that is the zero of the damping force set up by the molasses. A frequency chirp-cooled beam<sup>24</sup> loads the funnel with a 10% loading efficiency. The funnel generates a beam with density  $n$  of  $10^8 cm^{-3}$  at velocity  $v_z = 2.7 m/s$ . The authors report a longitudinal temperature of  $180 \mu K$  and a transverse temperature of  $300 \mu K$ , from which the brightness  $R$  and brilliance  $B$  are calculated to be  $3 \times 10^{15}$  and  $2 \times 10^{16} m^{-2} s^{-1} sr^{-1}$ , respectively. While the longitudinal temperature indicates a

low relative velocity along the beam direction, the larger transverse temperature corresponds to a transverse velocity spread greater than the longitudinal spread. To study collisional orientation and alignment effects a beam must have narrow laboratory divergence. The divergence of this beam does not provide an axis to which collisional effects can be referenced.

Nellessen, Werner, and Ertmer<sup>8</sup> developed a scheme to transversely compress a monoenergetic sodium beam. Atoms showed from a thermal source via chirp cooling are deflected from the hot background with near-resonant radiation. The slow, pulsed atom beam enters a region with a 2D MOT, which transversely cools and compresses the flux. The 2D MOT reduces the beam diameter from 3 mm to  $43 \mu m$ . The density of the compressed beam is on the order of  $10^9 cm^{-3}$ . The chirp-cooling method limits the longitudinal velocity spread to the Doppler absorption width ( $\sim 10 m/s$  for sodium), and they report a transverse velocity near the Doppler limit of 40 cm/s. The velocity distributions and density are of the same order as this experiment, but the flux is pulsed due to the chirp-cooling technique. The *peak* value of the brightness is  $5 \times 10^{21} m^{-2} s^{-1} sr^{-1}$  and the brilliance is  $1 \times 10^{23} m^{-2} s^{-1} sr^{-1}$ , however, the pulsed nature of the beam reduces the time-averaged values by the 10% duty cycle. The short existence of the bright beam reduces the signal to noise in experiments with low count rates, such as far-detuned ( $\Delta > 500 MHz$ ) photoassociative ionization.

A multistage collimation and brightening technique developed by Hoogerland *et al.*<sup>11</sup> increases the density of metastable neon beams. The system consists of the optical collimation of a thermal beam, followed by optical compression and secondary optical collimation stages. Because metastable noble gas beam sources are not as efficient as thermal alkali sources, the authors sacrifice mechanical divergence of the thermal beam to increase beam current. The maximum transverse component of atomic velocities exiting the source exceeds the Doppler capture range for a standing-wave molasses. A curved wave-front technique increases the transverse velocity capture range, increasing the number of atoms within the collimated beam. The collimated beam then passes through a 2D MOT that focuses toward the center of the trap. Residual transverse velocity gained in the compression stage is eliminated with a second collimation stage. Because the longitudinal distribution of atoms is broad, the chromatic aberration limits the density as the atoms are focused to different points. The brightness and brilliance are  $1 \times 10^{21}$  and  $6 \times 10^{21} m^{-2} s^{-1} sr^{-1}$ . The large longitudinal velocity spread (100 m/s) of the beam makes it unsuitable for cold collision studies. However, recent proposals<sup>12</sup> add a longitudinal slowing stage between the initial collimation and the compression stage that improves the prospects for cold collision study in metastable beams.

Lison *et al.*<sup>14</sup> recently demonstrated a very bright cesium beam. An effusive cesium beam is optically collimated and longitudinally cooled. A set of permanent magnets produce a large magnetic-field gradient that decouples the atoms from the cooling cycle, producing a narrow longitudinal velocity distribution. The atom beam then passes through a magnetic lens formed with a hexapole arrangement of permanent mag-

nets. The lens focuses the atoms to a point further downstream, where a near-resonant optical deflecting beam directs the atoms off-axis and into a collimating optical molasses stage. The longitudinal velocity is 35–120 m/s with a velocity spread of about 1 m/s. The brightness and brilliance are measured to be  $7 \times 10^{21}$  and  $7 \times 10^{23} \text{ m}^{-2} \text{ s}^{-1} \text{ sr}^{-1}$ . An advantage of this system over the one presented here is the lower laser power required by replacing the 2D MOT with a magnetic lens. Deflecting the cold beam off the original beam axis removes the atoms from the hot background flux and also from the influence of the longitudinal cooling laser.

A new system by Fukuyama *et al.*<sup>7</sup> that generates a bright, monoenergetic, pulsed lithium beam has recently been presented. Atoms collected in a magneto-optic trap are forced out of the trap by simultaneously blocking one of the trapping beams and temporally shifting the magnetic field. The magnetic-field shift compensates for the Doppler shift of the remaining trapping laser beams as the atoms accelerate out of the trapping region. The repetition rate of this source is 1 Hz, and the brightness of the flux is  $1.4 \times 10^{20} \text{ m}^{-2} \text{ s}^{-1} \text{ sr}^{-1}$ .

## V. DISCUSSION

We have produced a bright sodium beam, using a novel externally heated source to provide the initial flux, characterized by high density ( $1 \times 10^{10} \text{ cm}^{-3}$ ), low divergence ( $2 \times 10^{-6} \text{ sr}$ ), and a narrow longitudinal velocity distribution (5 m/s). The brightness of the atom beam is  $2 \times 10^{24} \text{ m}^{-2} \text{ s}^{-1} \text{ sr}^{-1}$ , the brightest to date. The beam has been used to study polarization effects in optical suppression collisions in sodium,<sup>17</sup> and we are currently using it to measure alignment and orientation effects in photoassociative ionization.<sup>18</sup> The low longitudinal velocity spread and high brightness also makes this beam technique useful for nanolithography and atom optic experiments.<sup>12–14</sup> This technique can be generalized to any of the alkali or metastable noble gas species and can be implemented with minor modifications to existing Zeeman cooling systems.

- <sup>1</sup>P. D. Lett, W. D. Phillips, S. L. Rolston, C. E. Tanner, R. N. Watts, and C. I. Westbrook, *J. Opt. Soc. Am. B* **6**, 2084 (1989).
- <sup>2</sup>J. R. Pierce, *Theory and Design of Electron Beams*, 2nd ed. (Van Nostrand, Princeton, NJ, 1954).
- <sup>3</sup>E. Riis, D. S. Weiss, K. A. Moler, and S. Chu, *Phys. Rev. Lett.* **64**, 1658 (1990).
- <sup>4</sup>J. Uy, J. Djemaa, P. Nosbaum, and P. Pillet, *Opt. Commun.* **112**, 136 (1994).
- <sup>5</sup>Z. T. Lu, K. L. Corwin, M. J. Renn, M. H. Anderson, E. A. Cornell, and C. E. Wieman, *Phys. Rev. Lett.* **77**, 3331 (1996).
- <sup>6</sup>K. Dieckmann, R. J. C. Spreeuw, M. Weidemüller, and J. T. M. Walraven, *Phys. Rev. A* **58**, 3891 (1998).
- <sup>7</sup>Y. Fukuyama, H. Kanou, V. I. Balykin, and K. Shimizu, *Appl. Phys. B: Lasers Opt.* **70**, 561 (2000).
- <sup>8</sup>J. Nellessen, J. Werner, and W. Ertmer, *Opt. Commun.* **78**, 300 (1990).
- <sup>9</sup>R. W. McGowan, D. M. Giltner, and S. A. Lee, *Opt. Lett.* **20**, 2535 (1995).
- <sup>10</sup>C.-C. Tsao, Y. Wang, J. Weiner, and V. S. Bagnato, *J. Appl. Phys.* **80**, 8 (1996).
- <sup>11</sup>M. D. Hoogerland, J. P. J. Driessen, E. J. D. Vredendregt, H. J. L. Megens, M. P. Schuwer, H. C. W. Beijerinck, and K. A. H. van Leeuwen, *Appl. Phys. B: Lasers Opt.* **62**, 323 (1996).
- <sup>12</sup>M. D. Hoogerland, D. Milic, W. Lu, H.-A. Bachor, K. G. H. Baldwin, and S. J. Buckman, *Aust. J. Phys.* **49**, 567 (1996).
- <sup>13</sup>R. E. Scholten, R. Gupta, J. J. McClelland, R. J. Celotta, M. S. Levenson, and M. G. Vangel, *Phys. Rev. A* **55**, 1331 (1997).
- <sup>14</sup>F. Lison, P. Schuh, D. Haubrich, and D. Meschede, *Phys. Rev. A* (to be published).
- <sup>15</sup>J. Weiner, V. S. Bagnato, S. Zilio, and P. S. Julienne, *Rev. Mod. Phys.* **71**, 1 (1999).
- <sup>16</sup>D. R. Herschbach, in *Advances in Chemical Physics*, edited by J. Ross (Interscience, New York, 1966).
- <sup>17</sup>W. DeGraffenreid, J. Ramirez-Serrano, Y.-M. Liu, A. Rosenbaum, and J. Weiner, *Appl. Phys. B: Lasers Opt.* (submitted).
- <sup>18</sup>J. Ramirez-Serrano, W. DeGraffenreid, Y.-M. Liu, and J. Weiner (unpublished).
- <sup>19</sup>J. Dalibard and C. Cohen-Tannoudji, *J. Opt. Soc. Am. B* **6**, 2023 (1989).
- <sup>20</sup>J. F. Kelly and A. Gallagher, *Rev. Sci. Instrum.* **58**, 563 (1987).
- <sup>21</sup>W. D. Phillips and H. Metcalf, *Phys. Rev. Lett.* **48**, 596 (1982).
- <sup>22</sup>R. J. Napolitano, S. C. Zilio, and V. S. Bagnato, *Opt. Commun.* **80**, 110 (1990).
- <sup>23</sup>E. M. Raab, M. Prentiss, A. Cable, S. Chu, and D. E. Pritchard, *Phys. Rev. Lett.* **59**, 2631 (1987).
- <sup>24</sup>W. Ertmer, R. Blatt, J. L. Hall, and M. Zhu, *Phys. Rev. Lett.* **54**, 996 (1985).